J. Biochem. **137**, 69–77 (2005)
DOI: 10.1093/jb/mvi010

Crystal Structure of Cold-Active Protein-Tyrosine Phosphatase from a Psychrophile, *Shewanella* sp.

Hiroki Tsuruta[1,*], Bunzo Mikami[2] and Yasuo Aizono[3]

[1]The Center for Innovation and Creativity, Kobe University, Kobe, Hyogo 657-8501; [2]Laboratory of Food Quality Design and Development, Division of Agronomy and Horticultural Science, Graduate School of Agriculture, Kyoto University, Gokasho, Uji, Kyoto 611-0011; and [3]Faculty of Agriculture, Kobe University, Kobe, Hyogo 657-8501

Received April 29, 2004; accepted October 26, 2004

The cold-active protein-tyrosine phosphatase (CAPTPase) of a psychrophile, *Shewanella* sp., shows high catalytic activity below 20°C. The catalytic residue of CAPTPase is histidine, as opposed to the cysteine of known protein-tyrosine phosphatases (PTPases), and the enzyme protein has three amino acid sequences, Asp-Xaa-His, Gly-Asp-Xaa-Xaa-Asp-Arg and Gly-Asn-His-Glu, that are observed in many protein-serine/threonine phosphatases (PS/TPases). We have determined the crystal structures of CAPTPase at 1.82 Å and the enzyme bound with a phosphate ion at 1.90 Å resolution using X-ray crystallography and the multiple isomorphous replacement method. The final refined models are comprised of 331 amino acid residues, two metal ions, 447 water molecules, and an acetate or phosphate ion in an asymmetric unit. The enzyme protein consists of three β-sheets, termed Sheet I, Sheet I′, and Sheet II, and 14 α-helices. The CAPTPase has a different overall structure from known protein-tyrosine phosphatases. The arrangement of two metal ions, a phosphate ion and the adjacent amino acid residues in the catalytic site of CAPTPase is identical to that of PS/TPases. Thus, it was confirmed that the CAPTPase was a novel PTPase with a conformation similar to the catalytic site of PS/TPase. We speculate that the hydrophobic moiety around the catalytic residue of CAPTPase might play an important role in eliciting high activity at low temperature.

Key words: cold-active enzyme, crystal structure, phosphoesterase motif, protein-serine/threonine phosphatase, protein-tyrosine phosphatase, *Shewanella* sp.

Abbreviations: CAPTPase, cold-active protein-tyrosine phosphatase; MIR, multiple isomorphous replacement; λPS/TPase, bacteriophage λ protein-serine/threonine phosphatase; PS/TPase, protein-serine/threonine phosphatase; PTPase, protein-tyrosine phosphatase.

Psychrophilic and ectothermic organisms constantly living in a low temperature environment have enzymes adapted to their environment. These enzymes, so called "cold-active enzymes," show higher catalytic activity at low and moderate temperatures, and lower thermostability than enzymes from mesophilic and thermophilic organisms (*1–3*). Cold-active enzymes have generated considerable interest, since they have potential as to improvement of the efficiency of industrial processes (*4*, *5*). Accumulation of fundamental information on the relationship between structure and function will facilitate application of these cold-active enzymes.

The enzymatical characteristics of cold-active enzymes may be attributed to their flexible structures (*6*). The three-dimensional structures of several cold-active enzymes have been determined using the molecular modeling method (*7–9*) and X-ray crystallography (*10*, *11*), and the structural features leading to the high flexibility have been speculated to be as follows: (i) reduced numbers of hydrogen bonds, salt bridges, isoleucine clusters and proline residues in loop regions; (ii) a low Arg/(Arg + Lys) content; and (iii) an increase in the number of glycine and serine residues close to their catalytic sites. Thermodynamic studies on thermal unfolding of the cold-active phosphoglycerate kinase of a psychrophile, *Pseudomonas* sp. TACII18, revealed that the cold-active enzyme is composed of heat-labile and heat-stable domains, these domains being involved in catalytic reactions and substrate-binding of this enzyme, respectively (*12*). Based on this observation, Lonhienne *et al.* proposed the notion of "local flexibility/rigidity," *i.e.* that acquisition of the flexible regions essential for the catalytic reaction and the rigid regions is important for increases in k_{cat} at low temperature (*13*). The detailed structural features leading to high catalytic activity at low temperature remained to be determined.

We isolated a CAPTPase from a psychrophile, *Shewanella* sp. (*14*). This enzyme showed high catalytic activity at low temperature and activation enthalpy below 20°C, which is much lower than that at intermediate temperatures above 20°C (*15*). PTPases, in general, contain an evolutionarily conserved segment of approximately 250 amino acid residues including the catalytic domain (*16*). Within this domain, there is a signature motif (His-Cys-Xaa-Ala-Gly-Arg, where Xaa indicates any amino acid). Mutational and chemical modifications have indicated that the invariant cysteine residue in this motif is essential for enzyme activity (*16*). The cysteine residue forms a

*To whom correspondence should be addressed. Tel: +81-78-803-5945, Fax: +81-78-803-5947, E-mail: tsuruta@kobe-u.ac.jp

Table 1. **Summary of phasing statistics.**

Heavy atom	Sodium tungstate	Merysalyl acid	Cadmium chloride
Data collection			
Wavelength (Å)	1.54	1.54	1.54
Resolution (Å)	2.67	3.0	2.51
Observed reflections	31,667	22,810	51,789
Unique reflections	9,869	7,495	12,109
Completeness (%)	91.0	96.9	94.8
R_{sym} (%)[a]	6.3	10.0	13.2
Redundancy	0.03	0.03	0.04
Phasing statistics			
Heavy atom sites	1	1	1
R_{cullis}[b]	0.52	0.63	0.72
R_{kraut}[c]	0.05	0.10 (0.14)[d]	0.09
Phasing power	1.93	1.24 (0.69)[d]	0.59
Mean figure-of-merit	0.823		

[a]$R_{sym} = \Sigma \mid I - \langle I \rangle \mid / \Sigma \langle I \rangle$, where I is the observed intensity of reflections. [b]$R_{cullis} = \Sigma \parallel F_{PH} \mid - \mid F_P \pm F_{H(calc)} \parallel / \Sigma \mid F_{PH} - F_P \mid$, [c]$R_{kraut} = \Sigma \parallel F_{derivative} \mid - \mid F_{native} + F_{H(calc)} \parallel / \Sigma \mid F_{derivative} \mid$, where F_{PH}, F_P and $F_{H(calc)}$ are the structural factor amplitudes for derivative, native and heavy atoms. [d]Values in parentheses were obtained from the anomalous contribution.

covalent bond to phosphate derived from the substrate as an intermediate in the catalytic reaction. The catalytic residue of the CAPTPase is histidine (*17*), and the enzyme protein has the three amino acid segments, Asp-Xaa-His, Gly-Asp-Xaa-Xaa-Asp-Arg and Gly-Asn-His-Asp/Glu (*18*), that are called the "phopshoesterase motif" and are observed in the PS/TPases of bacteriophage λ [λ PS/TPase] (*19*), rabbit muscle (*20*), and so on. Site-directed mutagenesis of histidine residues of the CAPTPase conserved in PS/TPases suggested that His150 serves as a general acid catalyst (*21*). The CAPTPase is a novel PTPase with the amino acid residues conserved in PS/TPases.

The flexibility needed for an efficient catalytic reaction at low temperature may be localized around the structure containing this histidine residue. We determined the three-dimensional structures of the CAPTPase and the phosphate (P_i)-bound enzyme using X-ray crystallography. The novelty and the structural features leading to the flexibility are discussed.

EXPERIMENTAL PROCEDURES

Protein Expression, Purification, and Crystallization—The gene of CAPTPase (*15*) was inserted between the *Nco*I and *Xho*I restriction sites of plasmid pET22b. *E. coli* AD494(DE3) was transformed with the resultant plasmid, *pTRCPTP*, to express the recombinant CAPTPase (*15*). The enzyme was purified as reported (*15*), *i.e.* by two step column chromatography on a Q-Sepharose FF column with a linear gradient of 0 to 0.3 M NaCl, followed by a hydroxylapatite column with stepwise elution with 150 mM sodium phosphate.

The hanging-drop vapor diffusion method (*22*) was used for crystallization. Crystals were grown in a drop of a protein solution (4.5 mg/ml) mixed with an equal volume of 0.1 M Tris-HCl buffer (pH 8.5) containing 30% (w/v) polyethyleneglycol 4000 as a precipitant and 0.2 M ammonium acetate as a salt, *i.e.* by a modification of the reported conditions (*23*). Crystals grew in one week at 4°C to reach 0.4 mm × 0.2 mm × 0.2 mm and had an octahedral shape (*23*).

Data Collection—An X-ray diffraction data set for a native crystal was collected to 1.82 Å resolution at 103 K with Cu*K*α radiation generated by a MAC Science M18XHF rotating anode generator on a Bruker HI-STAR multiwire area detector (*23*). The cell parameters and space group were determined to be $P2_12_12_1$ with a = 56.4 Å, b = 76.8 Å, c = 81.0 Å, and $\alpha = \beta = \gamma = 90°$. There is one molecule in an asymmetric unit, and approximately 46.2% of the crystal volume is occupied by solvent (*23*). The data sets for crystals soaked in 1 mM merysalyl acid, 2 mM sodium tungstate and 2 mM cadmium chloride were collected to 3.00, 2.67 and 2.51 Å, respectively. The data set for a crystal soaked in 0.1 M sodium phosphate buffer (pH 6.0) containing 30% (w/v) polyethyleneglycol 4000 and 0.2 M ammonium acetate was collected to 1.90 Å at 103 K. All data were processed and scaled using the program SAINT (Bruker).

Structure Determination and Refinement—The structure of the CAPTPase was determined using the MIR method and three isomorphous data sets plus the anomalous contribution of merysalyl acid (Table 1). Data scaling and map calculations were performed using the Phase 97 program package (*24*). The difference Patterson map calculations for merysalyl acid, sodium tungstate and cadmium chloride using data from 25–3.0 Å resolution allowed a clear interpretation of one heavy-atom site. Refinement of the heavy atom parameters and calculations of the initial phases were performed using with the program PHASIT (*25*). The resulting MIR map has a mean figure-of-merit of 0.546 at a resolution of 15 to 3.2 Å. The map was significantly improved by means of the solvent flattening process (*25*). The mean figure-of-merit reached 0.823 in the same resolution range. The initial model of the CAPTPase was built on the basis of the amino acid sequence and the solvent flattened MIR map using the program TURBO-FRODO (Architecture et Function des Macromolécules Biologiques-CNRS, Marseille, France) on an OCTANE computer (Silicon Graphics). For refinement of the protein model, the CNS pack-

Table 2. **Refinement statistics.**

	Native CAPTPase	P_i-bound CAPTPase
Resolution range used (Å)	15–1.82 (1.88–1.82)[e]	15–1.9 (1.97–1.90)[e]
Number of reflections	27,394 (1,592)[e]	23,327 (1,275)[e]
Completeness (%)	85.0 (50.1)[e]	82.4 (45.9)[e]
R-factor (%)[a]	17.8 (19.4)[e]	18.3 (24.7)[e]
R_{free}-factor (%)[b]	22.6 (24.4)[e]	23.5 (29.7)[e]
Average *B*-factors (Å)		
Overall	13.1	15.6
Protein	11.7	14.7
Waters	21.8	24.9
Metal ions	4.86	0.81
Acetate ion	24.2	–
Phosphate ion	–	18.1
R.M.S.D.[c] bond length (Å)	0.005	0.005
R.M.S.D.[c] bond angle (°)	1.3	1.3
Ramachandran geometry[d]		
Most favored (%)	88.1	88.1
Allowed (%)	10.5	10.5
Generously allowed (%)	0.3	0.3
Disallowed (%)	1.0	1.0
cis-peptide	1	1

[a]R-factor = $\Sigma \parallel F_{obs} \mid - \mid F_{calc} \parallel / \Sigma \mid F_{obs} \mid$. [b]An R_{free}-factor test set of 10% of the total reflections was used. [c]R.M.S.D., root mean square deviation. [d]Ramachandran geometry was monitored using PROCHECK (*27*). [e]Values in parentheses are the highest resolution shell.

age (*26*) was used. Rigid body refinement with the data between 15 and 4.0 Å resolution led to a decrease in the *R*-factor to 0.448. Refinement by stimulated annealing with molecular dynamics using a slow-cooling protocol from 3,000 K to 300 K yielded *R*-factor = 0.296. Several rounds of positional refinement and *B*-factor refinement, followed by manual model building, were carried out to try to improve the model. Water molecules were incorporated where the difference density had values of over 2.5 σ above the mean and the $2|F_o| - |F_c|$ map showed a density of more than 1 σ. When the crystal structure of the P_i-bound enzyme was determined, the refined model of the native CAPTPase was used as an initial model. The models were evaluated using PROCHECK (*27*). The figures in this paper were obtained using RASTER 3D (*28*), MOLSCRIPT (*29*), BOBSCRIPT (*30*), and GRASP (*31*).

Protein Data Bank Entry—The atomic coordinates of the CAPTPase have been deposited in the Protein Data Bank as entry 1V73.

RESULTS AND DISCUSSION

Quality of Model—The final model of the native CAPTPase comprised 331 amino acid residues, two metal ions, an acetate ion, and 447 water molecules in an asymmetric unit. The locations of the N-terminal five and C-terminal six amino acid residues were not included due to weak electron densities, and these residues were assumed to be disordered in the crystal structure. In the final model of the P_i-bound enzyme, one phosphate ion was bound near the position of the acetate ion in the native CAPTPase. The relevant refinement statistics are given in Table 2. The *R*- and R_{free}-factors of the final models were 0.178 and 0.226 for the native CAPTPase, and 0.183 and 0.235 for the P_i-bound CAPTPase, respectively. The r.m.s. deviation from ideality was 0.005 Å for bond lengths and 1.3° for bond angles. From a Luzzati plot (*32*), the mean absolute positional error was estimated to be 0.19 Å for the native CAPTPase and 0.21 Å for the P_i-bound CAPTPase, respectively. A Ramachandran plot (*33*) of the main-chain conformation angles of the native CAPTPase showed good geometry with 88.1% in the most favored region and 10.5% in the allowed region. Residues Asp117, Arg118, Asn201 and His286 lay outside the allowed regions. Asn201 lay within the ε region on the plot. This residue was located in the short hairpin turn structure consisting of four amino acid residues (Ile200–Val203). It is known that the second amino acid residue in this turn lies within the ε region due to the bond angle (*34*). There was one *cis*-peptide bond in the structure between Pro11 and Tyr12. The average *B*-factors of the native CAPTPase were calculated to be 11.7, 4.86, 24.2, and 21.8 Å^2 for protein, metal, acetate ion, and solvent atoms, respectively. And the value of the phosphate ion in P_i-bound CAPTPase was 18.1 Å^2.

The Overall Structure and Molecular Surface of CAPTPase—The CAPTPase molecule formed an ellipsoidal structure with dimensions of 47 Å × 46 Å × 52 Å. The enzyme protein was constructed of three β-sheets termed Sheet I, Sheet I′, and Sheet II, and 14 α-helices (Figs. 1 and 2). Sheet I′, which consisted of three anti-parallel β-strands, β1, β2 and β3, formed a small subdomain connected by a long loop containing αA, in the N-terminus. Sheet I comprised three parallel β-strands, β4, β5 and β6, and three anti-parallel β-strands, β12, β13 and β14. The parallel β-strands (β4–β6) formed a βαβαβ substructure with αB and αC. The residual five β-strands (β7–β11) formed Sheet II located in the face of Sheet I. Thirteen of the α-helices, the exception being for αA, surrounding Sheets I and II, could be separated into three-helix- (αB, αC and αN), four-helix- (αD–αG), and six-helix-bundles (αH–αM). The three-helix- and six-helix-bundles were

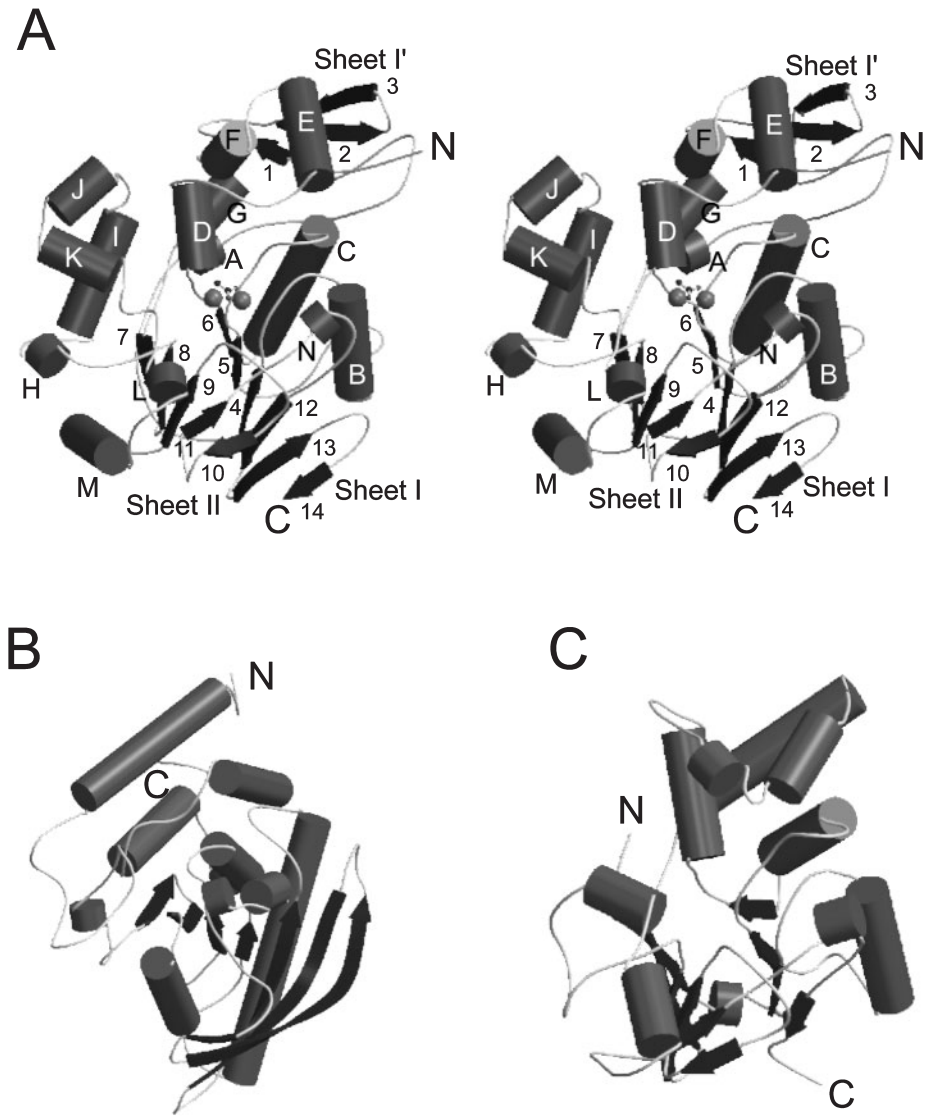

Fig. 1. **The overall structures of CAPTPase, and other PTPase and PS/TPase.** (A) The overall structure of native CAPTPase is shown as a stereo representation. Spheres represent metal ions. (B) and (C) show the overall structures of *yersinia* PTPase and λPS/TPase, respectively. α-Helices and β-strands are represented by cylinders and arrows, respectively.

flanked over the opposite side of Sheets I and II, respectively. The four-helix-bundle was located in the space surrounding the other two bundles and Sheet I′.

A narrow groove, ~30 Å long and ~5–8 Å wide, lay along the surface of CAPTPase (Fig. 3). The $|F_o| - |F_c|$ electron density map of P_i-bound CAPTPase calculated by removing the phosphate ion and the two metal ions (Fig. 4A) indicated that the two metal ions, the phosphate ion, and one solvent molecule were located in the deepest part of the groove. Although the species of the two metal ions could not be determined from the electron density map at 1.82 Å, the activity of the enzyme from which the metal ions had been removed increased remarkably in the presence of Mg^{2+} and Ca^{2+} ions, and slightly with Mn^{2+} ions (*14*). These findings indicated that Mg^{2+}, Ca^{2+}, and/or Mn^{2+} ions coordinated at the catalytic site. The presence of the phosphate ion suggested that the groove housed the catalytic site.

Comparison of the Overall Structures of CAPTPase, and Other PTPases and PS/TPases—CAPTPase can dephosphorylate phosphotyrosine, but not phosphoserine or phosphothreonine in proteins (*14*). To date, the crystal structures of several PTPases including human PTP1B (*35*), human SHP-2 (*36*), bovine low molecular weight PTPase (*37*), and *yersinia* PTPase (*38*) have been determined, and all PTPases have a highly twisted β-sheet structure. In the case of *yersinia* PTPase, the crystal structure (Fig. 1B) is composed of a single domain, with the polypeptide chain organized into 9 α-helices and 7 β-strands (*38*). The 7-stranded β-sheet that spans the entire length of the molecule adopts a highly twisted conformation. Moreover, cysteine as the catalytic residue of *yersinia* PTPase is located in the active center neighboring this β-sheet (*38*). CAPTPase does not have the twisted β-sheet, suggesting that CAPTPase has a different structure from known PTPases.

The catalytic residue of CAPTPase is histidine (*17*), and CAPTPase has the amino acid residues conserved in PS/TPases (*18*) (Fig. 2B). With regard to PS/TPases, the crystal structures of human protein phosphatase-1 (*39*, *40*), human calcineulin (*41*), and λPS/TPase (*42*) have been reported. These data provided evidence that PS/TPases have a βαβαβ substructure and the following α-helix as a common structural feature, and the conserved

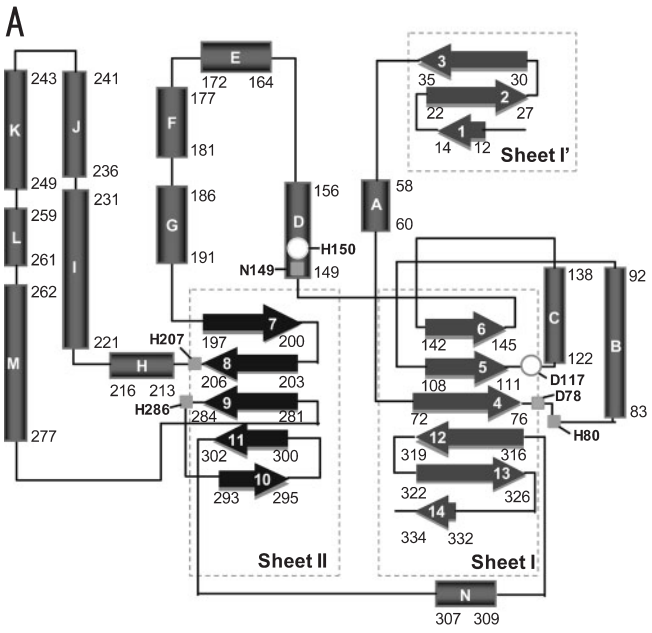

Fig. 2. **Secondary structure diagram (A) and the conserved amino acid residues (B) of CAPTPase.** (A) α-Helices and β-strands are represented by boxes and arrows, respectively. Numbers indicate the residue numbers at the beginning and end of the respective secondary structures. Circles and squares represent the residues (His150 and Asp117) essential for the catalysis and those involved in the binding of metal ions, respectively. (B) Each amino acid is shown in a one-letter code. The numbers above the alignments correspond to the amino acid numbers for the N-terminus of CAPTPase expressed in *E. coli*. Asterisks indicate amino acids identical in all phosphatases. Dark and light grey represent α-helix D, and β-strands 4, 5, and 6 of CAPTPase, respectively. CAPTPase, cold-active protein-tyrosine phosphtase (*18*); lamPPase, bacteriophage λ protein-phosphatase (*19*); Prp A and PrpB, *E. coli* phosphoprotein phosphatases (*38*); PyPP1, *P. abyssi* protein-serine/threonine phosphatase (*39*); PP1arch, *S. solfataricus* protein-serine/threonine phosphatase (*40*); PPZ, *S. cerevisiae* phosphoprotein phosphatase PP-Z1 (*41*).

amino acid residues, the phosphoesterase motif, in the substructure forms part of the catalytic site of PS/TPases. λPS/TPase is the smallest molecule among PS/TPases with the common substructure (*42*). As shown in Fig. 1C, the overall structure of λPS/TPase (*35*) comprises two β-sheets (4- and 6-stranded), and 6 long and 4 short α-helices. Three β-strands in the 4-stranded β-sheet form the βαβαβ substructure with 2 α-helices. CAPTPase has the substructure (β4, αB, β5, αC, and β6) and the following α-helix (αD) (Fig. 1A), and the conserved amino acid residues are positioned at the C-termini of β4 (residues

Table 3. **Distances among protein ligands, acetic acid/phosphate ions and metal ions.**

	Distance (Å)	
	Native CAPTPase	P_i-bound CAPTPase
M1–M2	3.4	3.5
M1–Asp78 Oδ1	2.0	2.0
M1–His80 Nε2	2.1	2.1
M1–Asp114 Oδ1	2.2	2.1
M1–Wat1 O	2.1	–
M1–Wat2 O	2.2	2.1
M2–Asn149 Nδ2	2.0	2.0
M2–His207 Nε2	2.0	2.0
M2–His286 Nδ1	2.2	2.2
M2–Asp114 Oδ1	2.4	2.4
M2– Wat1 O	2.1	–
Acetate O1–M1	2.7	–
Acetate O1–Arg118 Nγ2	2.9	–
Acetate O2–Arg258 Nγ1	2.8	–
Phosphate O1–M1	–	2.0
Phosphate O1–M2	–	2.2
Phosphate O2–M2	–	3.0
Phosphate O2–Asn149 Oδ1	–	2.8
Phosphate O2–His150 Nε2	–	2.8
Phosphate O3–M1	–	3.3
Phosphate O3–Arg118 Nγ1	–	2.8
Phosphate O4–Arg258 Nγ1	–	2.7

Asp78 and His80) and β5 (residues Gly113, Asp114 and Asp117), and in αD (residues Gly148, Asn149, His150 and Gln151) (Fig. 2). Accordingly, CAPTPase has a structure common to PS/TPases but not PTPases, although the overall structure is not similar to that of λPS/TPase.

Catalytic Site of CAPTPase—The catalytic site of CAPTPase was formed by the two metal ions, residues Asp78, His80, Asp114, Asp117 and Asn149 from the βαβαβ substructure, residue His150 from αD, and residues His207 and His286 located in the loops at the C-termini of β8 and β9, respectively (Fig. 4A). Each of the metal ions in the native CAPTPase was coordinated by six ligands in a tetrahedral bipyramidal arrangement (M1) and by five ligands in a pentahedral arrangement (M2), respectively. In P_i-bound CAPTPase, however, both metal ions had tetrahedral bipyramidal coordination with six ligands. The distances among amino acid residues, metal ions, and acetate or phosphate ions in the catalytic sites of the native and P_i-bound CAPTPases are summarized in Table 3. In the case of native CAPTPase, M1 was coordinated by His80 Nε2, a single carboxylate oxygen atom of Asp78, an oxygen atom of the acetate ion, and two water molecules (Wat1 and Wat2). The uncoordinated side chain oxygen atom of Asp78 was hydrogen bonded to His286 N. M2 was coordinated by His207 Nε2, His286 Nδ1, Asn149 O, and Wat1. Asp114 Oδ1 was coordinated to both metal atoms with its uncoordinated side chain oxygen atom (Oδ2) hydrogen bonded to His150 N. M1 and M2 in P_i-bound CAPTPase were coordinated to the phosphate O1 located at the position of Wat1 O in the native CAPTPase.

As shown in Fig. 4B, the arrangement of the seven amino acid residues (Asp78, His80, Asp114, Asn149, His150, His207 and His286), metal ions and a phosphate

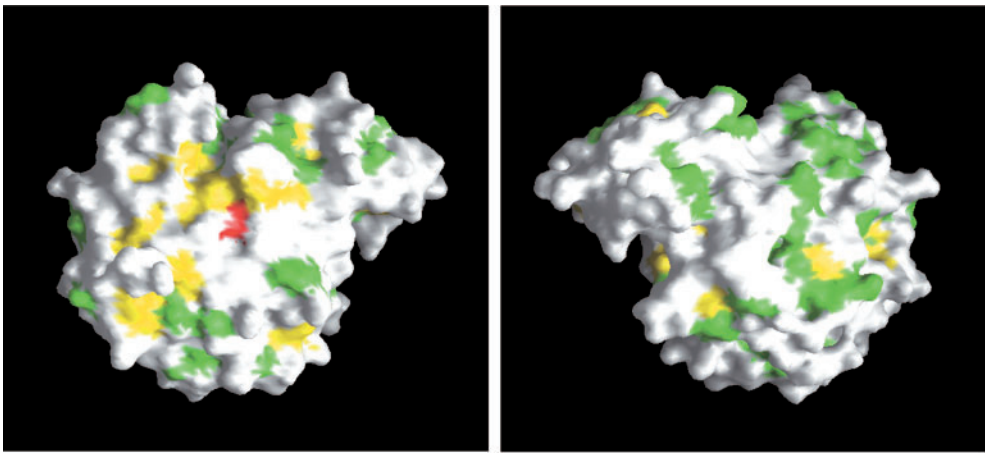

Fig. 3. **Moleculer surface of CAPTPase.** The right-hand view shows the left-hand view rotated by 180°. Metal ions in the catalytic site are shown in red. The aromatic and hydrophobic residues on the surface of CAPTPase are colored yellow and green, respectively.

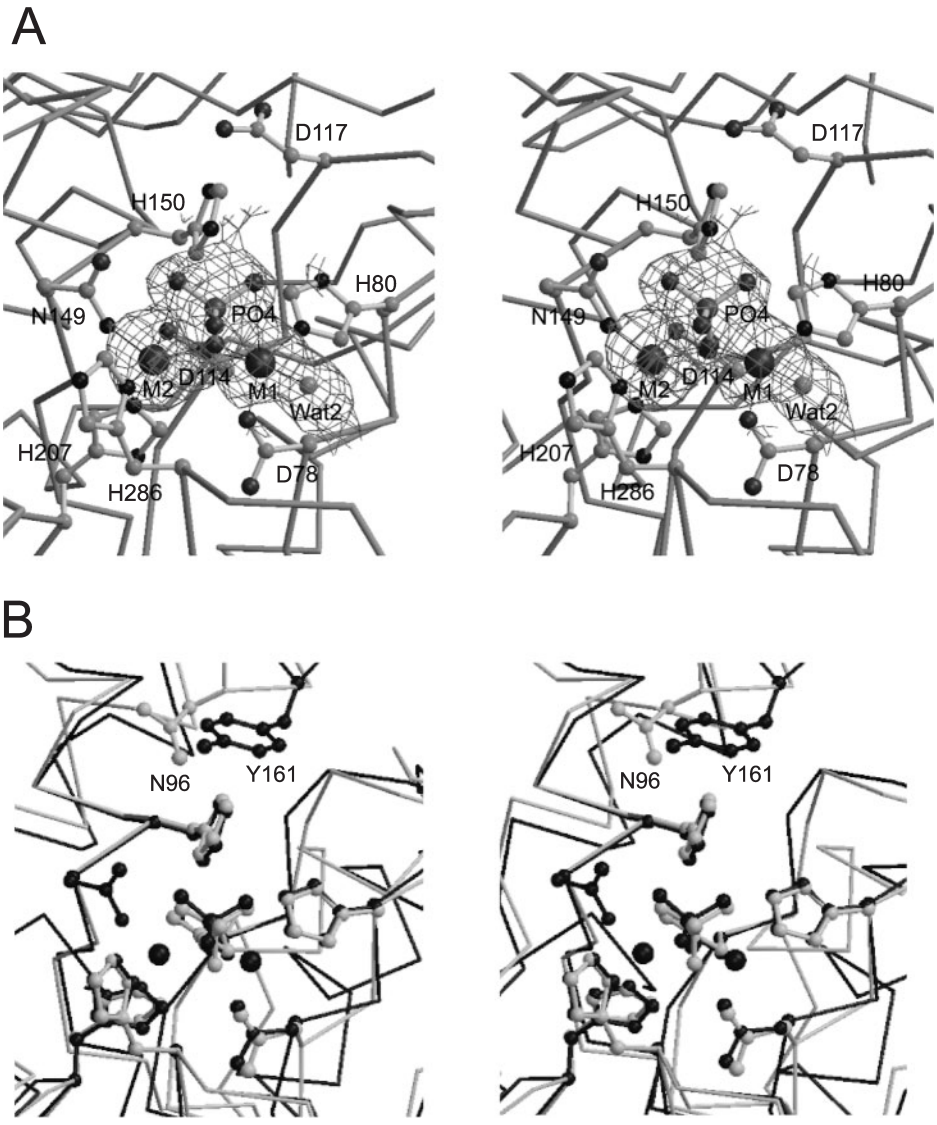

Fig. 4. **Stereoviews of the catalytic site of P_i-bound CAPTPase.** (A) The side chains of the residues essential for the catalytic reaction and metal binding are represented on the main chain. Large spheres indicate metal ions. An $|F_o| - |F_c|$ omit map around the phosphate and metal ions is plotted at +1.5σ. (B) The main chains and side chains of the amino acid residues, phosphate/sulfate ions, and metal ions, which are located at the catalytic sites of P_i-bound CAPTPase and λPS/TPase, are shown in black and grey, respectively, as a stereo representation.

ion in the P_i-bound CAPTPase molecule was identical to that of the corresponding residues, metal ions and a sulfate ion in the λPS/TPase molecule. The r.m.s.d. for 50 Cα atoms of amino acids including the seven conserved residues, phosphorus atom, and metal atoms is 0.58 Å. Also, Asp117, Arg118 and His286, which were located in the catalytic site of CAPTPase, lay outside the allowed regions on the Ramachandran plot. The corresponding three residues in λPS/TPase also lie within the disallowed region on the plot. Therefore, CAPTPase is a novel

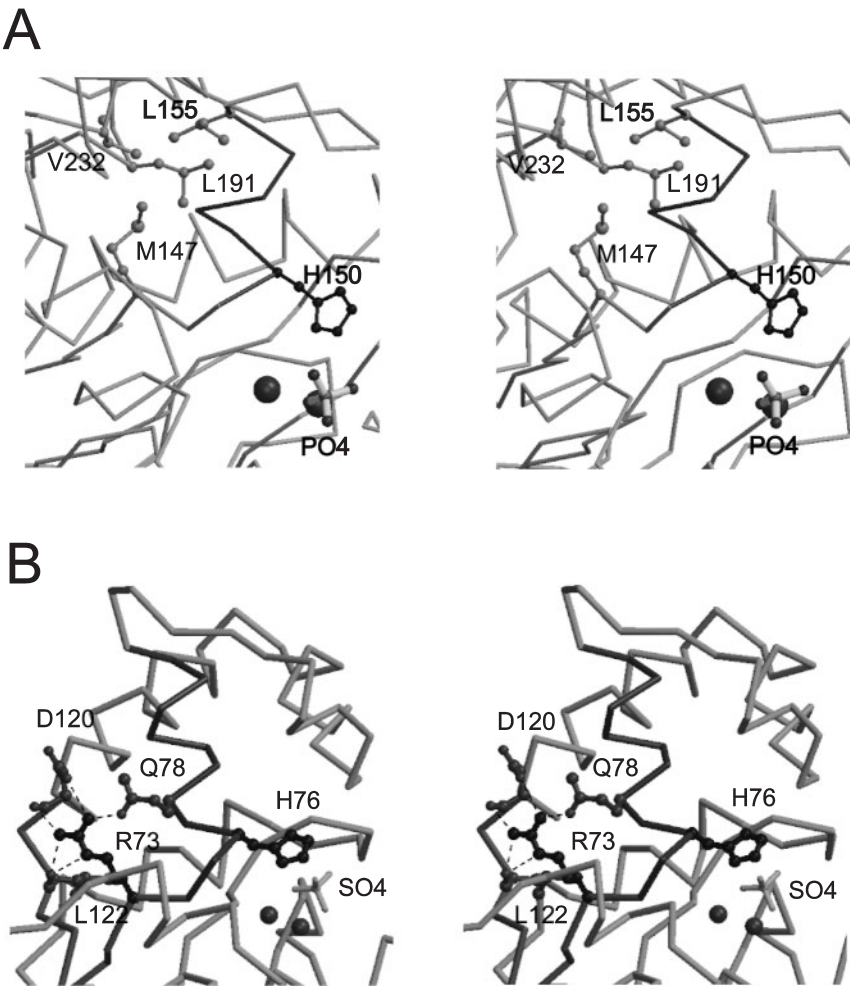

Fig. 5. **Stereoviews of the loop structures located behind the catalytic sites of CAPTPase and λPS/TPase.** (A) The structure around αD (dark grey) of CAPTPase is shown with the side chains of Met147, Leu155, Leu191 and Val232 (light grey), and His150 (black). (B) The structure of λPS/TPase is shown with the side chains of Gln78, Asp120, Leu122, Arg73 and His76 (black). The latter histidine residue corresponds to His150 in CAPTPase. Spheres are metal ions in CAPTPase and λPS/TPase.

PTPase with a conformation similar to the catalytic site of PS/TPases.

Substrate Specificity—Since P_i-bound CAPTPase and λPS/TPase had identical catalytic site structures (Fig. 4B), dephosphorylation of the respective substrates might also proceed through similar mechanisms. CAPTPase, however, could dephosphorylate phosphotyrosine residues but not phosphoserine or phosphothreonine ones (*14*). Tyrosine exhibits a different size and hydrophobicity of the side chain from serine and threonine, suggesting that CAPTPase possesses structural features that preferentially recognize tyrosine. As shown in Fig. 4B, in the region neighboring the catalytic site, probably the substrate-binding site of this enzyme, the phenyl ring of Tyr161 was located, whereas Asn96 was located at the corresponding position in λPS/TPase (*42*). This suggested that the phenyl ring of Tyr161 plays a key role in the substrate-recognition of CAPTPase. Furthermore, the groove adjacent to the catalytic site is formed by αI and the loop connecting αK and αL on one side, and by αD on the other side. On the wall, the side chains of the aromatic amino acid residues, Phe249, Phe250, and Trp256, were distributed. The groove in the PS/TPase molecule may contain the substrate binding site (*43*), and the major constituents of the wall are the side chains of hydrophobic amino acid residues. Differences in the types of amino acid residues constituting the wall of the groove may reflect differences in the recognized substrate polypeptides between CAPTPase and λPS/TPase.

Speculation of Structural Properties for Eliciting High Activity at Low Temperature—Our view is that the flexibility that could account for the high catalytic activity of CAPTPase at low temperature is localized around the structure containing amino acid residues essential for the catalysis. The catalytic site of CAPTPase is mainly constructed through hydrophobic interaction. In particular, CAPTPase possesses distinctive feature(s) in the conformation around the catalytic residue, His150. In the loop between β6 and αD, the side chain of Met147 in cold-active PTPase is located in the surrounding space with the side chains of hydrophobic amino acid residues including Leu155, Leu191, and Val232 in the range of ~5 Å (Fig. 5A). In contrast, in the corresponding loop of λPS/TPase (*42*), the leucine and glycine residues are conserved, but the arginine residue Arg73 is located at the position of Met147 in CAPTPase (Fig. 2B). As shown in Fig. 5B, the nitrogen atoms of Arg73 form five hydrogen bonds to the oxygen atoms in the side chains of the surrounding residues, Arg73 Nγ1 to Gln78 Oε1, Arg73 Nγ1 to Asp120 Oδ1, Arg73 Nγ2 to Asp120 O, and Arg73 Nγ2 and Nε to Leu122 O (*35*). In general, a hydrophobic interaction is relatively weaker than a combination of hydrogen

bonds (*44*). Therefore, maintenance of the conformation of the catalytic site through the hydrophobic interaction mediated by Met147 could be one factor accounting for the flexibility of the loop before αD, which may provide the motility with a particular direction to αD containing His150 at low temperature. The details of the mechanisms involved in elicitation of high catalytic activity at low temperature will be revealed on determination of the crystal structure of the CAPTPase-substrate complex, and mutation of the residues essential for the flexibility of the PTPase has to be performed.

This study was supported in part by a Grant from the Japan Foundation for Applied Enzymology.

REFERENCES

1. Devail, S., Feller, G., Narinx, E., and Gerday, Ch. (1994) Cold adaptation of proteins. *J. Biol. Chem.* **267**, 17448–17453
2. Rentier-Delrue, F., Mande, S.C., Moyens, S., Terpstra, P., Mainford, V., Gorai, K., Lion, M., Hol, W.G.J., and Martial, J.A. (1993) Cloning and overexpression of the triosephosphate isomerase genes from psychrophilic and thermophilic bacteria. *J. Mol. Biol.* **229**, 85–93
3. Arpigny, J.L., Feller, G., and Gerday, Ch. (1993) Cloning, sequence and structural features of a lipase from psychrophile *Psychrobacter immbolis* B10. *Biochim. Biophys. Acta* **1171**, 331–333
4. Cavicchioli, R., Siddiqui, K.S., Andrews, D., and Sowers, K.R. (2002) Low-temperature extremophiles and their applications. *Curr. Opin. Biotech.* **13**, 253–261
5. Gerday., Ch., Aittaleb, M., Bentahir, M., Chessa, J-P., Claverie, P., Collins, T., D'Amico, S., Dumont, J., Garsoux, G., Georelette, D., Hoyoux, A., Lonhienne, T., Meuwis, M-A., and Feller, G. (2000) Cold-adapted enzymes: from fundamentals to biotechnology. *Trends Biotechnol.* **18**, 103–107
6. Feller, G., Narinx, E., Aprigny, J.L., Aittaleb, M., Baise, E., Genicot, S., and Gerday, Ch. (1989) Enzymes from psychrophilic organisms. *FEMS Microbiol. Rev.* **18**, 189–202
7. Feller, G., Dayan, F., Theys, F., Qian, M., Hasen, R., and Gerday, Ch. (1994) Stability and structure analysis of α-amylase from the Antarctic psychrophile *Alteromonas haloplanctis* A23. *Eur. J. Biochem.* **222**, 441–447
8. Arpigny, J.L., Lamotte, J., and Gerday, Ch. (1997) Molecular adaptation to cold of an Antarctic bacterial lipase. *J. Mol. Catal. B* **3**, 29–35
9. Narinx, E., Baise, E., and Gerday, Ch. (1997) Subtilisin from psychrophilic Antarctic bacteria: characterization and site-directed mutagenesis of residues possibly involved in the adaptation to cold. *Protein Eng.* **10**, 101–109
10. Aghajari, N., Feller, G., Gerday, Ch., and Haser, R. (1998) Structures of the psychrophile *Alteromonas haloplanctis* α-amylase give insights into cold adaptation at a molecular level. *Structure* **6**, 1503–1506
11. Russel, R.J.M., Gerike, U., Danson, M.J., Hough, D.W., and Taylor, G.L. (1998) Structural adaptations of the cold-active citrate synthase from an Antarctic bacterium. *Structure* **6**, 351–361
12. Bentahir, M., Feller, G., Aittaleb, M., Lamotte-Brasseur, J., Himri, T., Chessa, J.P., and Gerday, Ch. (2000) Structural, kinetic and calorimetric characterization of the cold-active phosphoglycerate kinase from the Antarctic *Pseudomonas* sp. TACII18. *J. Biol. Chem.* **275**, 11147–11153
13. Lonhienne, T., Gerday, Ch., and Feller, G. (2000) Psychrophilic enzymes:revising the thermodynamic parameters of activation may explain local flexibility. *Biochim. Biophys. Acta* **1543**, 1–10
14. Tsuruta, H., Tsuneta, S.T., Ishida, Y., Watanabe, K., Uno, T., and Aizono, Y. (1998) Purification and some characteristics of phosphatase of a psychrophile. *J. Biochem.* **123**, 219–225
15. Tsuruta, H. and Aizono, Y. (2003) Catalytic efficiency and some structural properties of cold-active protein-tyrosine-phosphatase. *J. Biochem.* **133**, 225–230
16. Walton, K.M. and Dixon, J.E. (1990) Protein tyrosine phoshatases. *Annu. Rev. Biochem.* **62**, 101–120
17. Tsuruta, H. and Aizono, Y. (1999) Enzymatical properties of psychrophilic phosphatase I. *J. Biochem.* **125**, 690–695
18. Tsuruta, H. and Aizono, Y. (2000) Cloning of phosphatase I gene from a psychrophile, *Shewanella* sp., and some properties of the recombinant enzyme. *J. Biochem.* **127**, 143–149
19. Cohen, P.T.W. and Cohen, P. (1989) Discovery of a protein phosphatase activity encoded in the genome of bacteriophage λ: Probable identity with open reading frame 221. *Biochem. J.* **260**, 931–934
20. Cohen, P.T.W. (1988) Two isoforms of protein phosphatase 1 may be produced from the same gene. *FEBS Lett.* **232**, 17–23
21. Tsuruta, H., Tamura, J., Yamagata, H., and Aizono, Y. (2004) Specification of amino acid residues essential for the catalytic reaction of cold-active protein-tyrosine phosphatase of a psychrophile, *Shewanella* sp. *Biosci. Biotechnol. Biochem.*, **68**, 440–443
22. McPherson, A. (1985) Crystallization of macromolecules: general principles. *Methods Enzymol.* **114**, 112–120
23. Tsuruta, H., Mikami, B., Yamamoto, C., and Aizono, Y. (2002) Crystallization and preliminary x-ray studies of cold-active protein-tyrosine phosphatase of *Shewanella* sp. *Acta Crystallogr. D* **58**, 1465–1466
24. Furey, W. and Swaminathan, S. (1997) PHASES-95: a program package for processing and analyzing diffraction data from macromolecules. *Methods Enzymol.* **277**, 590–620
25. Wang, B.C. (1985) Resolution of phase ambiguity in macromolecular crystallography. *Methods Enzymol.* **115**, 90–112
26. Brunger, A.T., Adams, P.D., Clore, G.M., DeLano, W.L., Gros, P., Grosse-Kunstleve, R.W., Jiang, J.S., Kuszewski, J., Nilges, M., Pannu, N.S., Read, R.J., Rice, L.M., Simonson, T., and Warren, G.L. (1998) Crystallography & NMR system: a new software suite for macromolecular structure determination. *Acta Crystallogr. D* **54**, 905–921
27. Kraulis, P.J. (1991) MOLSCRIPT: a program to produce both detailed and schematic plots of protein structures. *J. Appl. Crystallog.* **24**, 946–950
28. Laskowski, R.A., MacArthur, M.W., Moss, D.S., and Thornton, J.M. (1993) PROCHECK: a program to check the stereochemical quality of protein structures. *J. Appl. Crystallog.* **26**, 283–291
29. Merritt, E.A. and Murphy, M.E.P. (1994) RASTER 3D version 2.0 a program for photorealistic molecular graphics. *Acta Crystallogr. D* **50**, 869–873
30. Esnouf, R.M. (1997) An extensively modified version of Molscript that includes greatly enhanced coloring capabilities. *J. Mol. Graphics* **14**, 132–134
31. Nicholls, A. and Honig, B. (1991) A rapid finite difference algorithm, utilizing successive over relaxation to solve the Poisson-Boltzmann equation. *J. Comput. Chem.* **12**, 435–445
32. Luzzati, V. (1952) Traitment statistique des erreurs dans la determination des structures cristallines. *Acta Crystallogr.* **5**, 802–810
33. Ramachandran, G.N., Ramakrishnan, C., and Sasisekharan, V. (1963) Stereochemistry of polypeptide chain configurations. *J. Mol. Biol.* **7**, 95–99
34. Efimiv, A.V. (1997) Structural trees for protein superfamilies. *Proteins* **28**, 245–260
35. Barford, D., Flint, A.J., and Tonks, N.K. (1994) Crystal structure of human protein tyrosine phosphatase 1B. *Science* **263**, 1397–1404
36. Hof, P., Pluskey, S., Dhe-Paganon, S., Eck, M.J., and Shoelson, S.E. (1998) Crystal structure of the tyrosine phsphatase SHP-2. *Cell* **92**, 441–450
37. Zhang, M., Stauffacher, C.V., Lin, D., and Van-Etten, R.L. (1998) Crystal structure of a human low molecular weight phosphotyrosyl phosphatase. *J. Biol. Chem.* **273**, 21714–21720

38. Fauman, E.B., Yuvaniyama, C., Schubert, H.L., Stuckey, J.A., and Saper, M.A. (1996) The x-ray crystal structures of *Yersinia* tyrosine phosphatase with bound tungstate and nitrate. *J. Biol. Chem.* **271**, 18780–18788
39. Goldberg, J., Huang, H.B., Kwon, Y.G., Greengard, P., Narin, A.C., and Kuriyan, J. (1995) Three dimensional structure of the catalytic subunit of protein serine/threonine phosphatase-1. *Nature* **376**, 745–753
40. Egloff, M.P., Cohen, P.T., Reinemer, P., and Barford, D. (1995) Crystal structure of the catalytic subunit of human protein phosphatase1 and its complex with tungstate. *J. Mol. Biol.* **254**, 942–959
41. Griffith, J.P., Kim, J.L., Kim, E.E., Sintchak, M.D., Thomson, J.A., Fitzgibbon, M.J., Fleming, M.A., Caron, P.R., Hsiao, K., and Navia, M.A. (1995) X-ray structure of calcineurine inhibited by the immunophilin-immunosupressant FKBP12-F506 complex. *Cell* **82**, 507–522
42. Voegtli, W.C., White, D.J., Reiter, N.J., Rusnak, F., and Rosenzweig, A.C. (2000) Structure of the bacteriophage λ ser/thr phosphatase with sulfate ion bound in two coordination modes. *Biochemistry* **39**, 15365–15374
43. Maynes, J.T., Bateman, K.S., Cherney, M.M., Das, A.K., Luu, H.A., Holmes, C.F.B., and James, M.N.G. (2001) Crystal structure of the tumor-promoter okadaic acid bound to protein phosphatase-1. *J. Biol. Chem.* **47**, 44078–44082
44. Fersht, A. (2000) *Structure and Mechanism in Protein Sci.: A Guide to Enzyme Catalysis and Protein Folding*, W.H. Freeman and Company, New York
45. Missiakas, D. and Raina, S. (1997) Signal transduction pathways in response to protein misfolding in the extracytoplasmic compartments of *E. coli*: role of two new phosphoprotein phosphatase PrpA and PrpB. *EMBO J.* **16**, 1670–1685
46. Mai, B., Frey, G., Swanson, R.V., Mathur, E.J., and Stetter, K.O. (1998) Molecular cloning and functional expression of a protein-serine/threonine phosphatase from the hyperthermophilic archaeon *Pyrodictium abyssi* TAG11. *J. Bacteriol.* **180**, 4030–4035
47. Leng, J., Cameron, A.J.M., Buckel, S., and Kennelly, P.J. (1995) Isolation and cloning of a protein-serine/threonine phosphatase from an archaeon. *J. Bacteriol.* **177**, 6510–6517
48. Posas, F., Casamayor, A., Morral, N., and Arino, J. (1992) Molecular cloning and analysis of a yeast protein phosphatases with an unusual amino-terminal region. *J. Biol. Chem.* **267**, 11734–11740